Adjoint-Based Sonic Boom Reduction for Wing-Body Configurations in Supersonic Flow

Siva K. Nadarajah * Antony Jameson ** Juan Alonso **

Abstract

This paper presents an adjoint method for the calculation of remote sensitivities in supersonic flow. The goal is to develop a set of adjoint equations and their corresponding boundary conditions to quantify the influence of geometry modifications on the pressure distribution at an arbitrary location within the domain of interest, away from the surface of the aircraft. First, this paper presents the formulation and discretization of the adjoint equations. The special treatment of the adjoint boundary condition to obtain remote sensitivities is also discussed. Second, we present results that demonstrate the application of the theory to a three-dimensional remote inverse design problem using a supersonic business jet wing-body configuration.

Résumé

Dans cet article, nous présentons une méthode adjointe de calcul des sensibilités à distance dans le flot supersonique. L'objectif est la mise au point d'une série d'équations adjointes et de leurs conditions aux limites correspondantes, afin de quantifier l'influence des modifications de la géométrie sur la distribution de la pression à une position arbitraire dans le domaine d'intérêt,

continued on page 188

NOMENCLATURE

A	flux Jacobian matrix
$\mathcal{B}$	boundary
C	non-dimensional coefficient
c	chord length
$\mathcal{D}$	domain
D	discrete adjoint artificial dissipation flux
d	artificial dissipation flux
E	internal energy
$\mathcal{F}$	design variable
F	Euler numerical flux vector
FF	far field
f	Euler flux vector
G	gradient
G	smoothed gradient
h	numerical flux across cell interface
I	cost function
n	outward normal
p	pressure
q	flux velocity
R	residual
$\mathcal{S}$	shape function
S	face areas of computational cell
s	arc length
T	temperature
t	time
U	scaled contravariant velocity component
u	velocity (physical domain)
w	state vector
x	coordinates (physical domain)
z	altitude
α	angle of attack
ϵ	adjustable constant for artificial dissipation scheme
Λ	numerical spectral radius of the flux Jacobian matrix
λ	spectral radius of the flux Jacobian matrix
ξ	coordinates (computational domain)

* CFD Laboratory
Department of Mechanical Engineering
McGill University
688 Sherbrooke Street West, Room 711
Montreal, QC H3A 2S6, Canada.

** Department of Aeronautics and Astronautics
Stanford University
Durand Building, 496 Lomita Mall
Stanford, CA 94305, USA
E-mail: siva.nadarajah@mcgill.ca

Received 12 April 2005

suite de la page 187

à distance de la surface de l'avion. Cet article présente, premièrement, la formulation des équations adjointes et leur dicrétisation. Nous y discutons également du traitement spécial de la condition aux limites adjointe permettant de dériver les sensibilités à distance. En second lieu, nous montrons l'application de la théorie à un problème inverse tridimensionnel de conception tenant compte des effets à distance, visant la configuration du fuselage et des ailes d'un réacté d'affaires supersonique.

ρ	density
ψ	Lagrange multiplier
ϖ	weighting coefficients

Subscripts

$\mathcal{I}$	contributions associated with variation of the state vector
$\mathcal{II}$	contributions associated with variation of the shape function
D	drag
i, j, k	cell indices
I	contributions associated with variation of the state vector
II	contributions associated with variation of the shape functions
max	maximum index
NF	near field
T	target
W	wall
+, –	cells across the cell face

INTRODUCTION

A 2001 US National Research Council study (Committee on Breakthrough Technology for Commercial Supersonic Aircraft 2001) concluded that, "… the sonic boom is the major barrier to the development of the supersonic business jet and a major, but not the only, barrier to the development of supersonic transports with overland capability". The Committee also determined that there was a potential market for at least 200 supersonic business jets over a 10-year period. The 8–15 passenger jets will probably fly at approximately Mach 1.8 with a range of 3000–4000 nautical miles (1 nautical mile = 1.852×10^3 m).

Concorde, a commercial supersonic aircraft built by France and Britain was in operation for more than 30 years. It cruised at Mach 2.0 with a total range of 4090 nautical miles at 60 000 ft (1 ft = 3.048×10^{-1} m) and consumed 6200 gallons of fuel per hour (1 gallon = 4.54609×10^{-3} m^3). The aircraft retired from commercial service on the 24 October 2003 due to both commercial and technical factors. The new breed of supersonic transports must possess superior performance characteristics apart from low sonic boom capability, compared to its predecessors to compete in the commercial jet industry. These include improvements in structures, aerodynamics, and propulsion. In particular, the experience of NASA's HSR program suggests that it should be possible to improve the lift-to-drag ratio from the value of 7.5 attained by the Concorde to around 9 (Cliff et al., 2001). Designs of supersonic transports of the future will benefit from multidisciplinary optimization techniques that were not available during the design and construction of aircraft like the Concorde.

Before the sonic boom reduction problem can be attempted, it is important to have the capability of calculating the sonic boom or ground pressure signature accurately. For typical cruise altitudes required for aircraft efficiency, the distance from the source of the acoustic disturbance to the ground is typically greater than 50 000 ft. A reasonably accurate propagation of the pressure signature can only be obtained with small computational mesh spacings that would render the analysis of the problem intractable for even the largest parallel computers. An approach that has been used successfully in the past is the use of near-to-far field extrapolation of pressure signatures based on principles of geometrical acoustics and non-linear wave propagation. These methods are based on the solutions of simple ordinary differential equations for the propagation of the near-field pressure signature to the ground. The Whitham F-function (Whitham, 1952) and Thomas' equivalent wave-form parameter method (Thomas, 1972) are common methods of choice.

Figure 1 is a schematic of the propagation of the aircraft pressure signature. "CFD Far Field" indicates the far-field boundary of the mesh. At a pre-specified distance below the aircraft and still within the CFD mesh, the location of a near-field plane can be seen. This plane is the effective interface between the CFD solution and the wave propagation program. At the near-field plane, the flow solution w_o is represented using a number of parameters, M, which can be taken, for example, as the number of mesh points on which the pressure wave-form has a value significantly different from the free stream. The lower portion of the domain between the CFD near field and the ground plane is where the pressure signature propagation method will be active. Given the conditions, w_o, the propagation altitude, and the altitude-dependent atmospheric properties $\rho(z)$, $p(z)$, $T(z)$, the propagation method produces a pressure signature at the ground plane we are interested in, which can be used to determine any of a variety of measures of sonic boom impact such as overpressures, rise time, impulse, etc.

Traditional methods to reduce the sonic boom signature target aircraft weight reduction, increases in lift-to-drag ratio, better specific fuel consumption, etc. Seebass and Argrow (1998) revisited sonic boom minimization and provided a detailed study of sonic boom theory and figures of merit for the level of sonic booms. Diverse methods have been employed in the design of low-boom aircraft configurations. The following

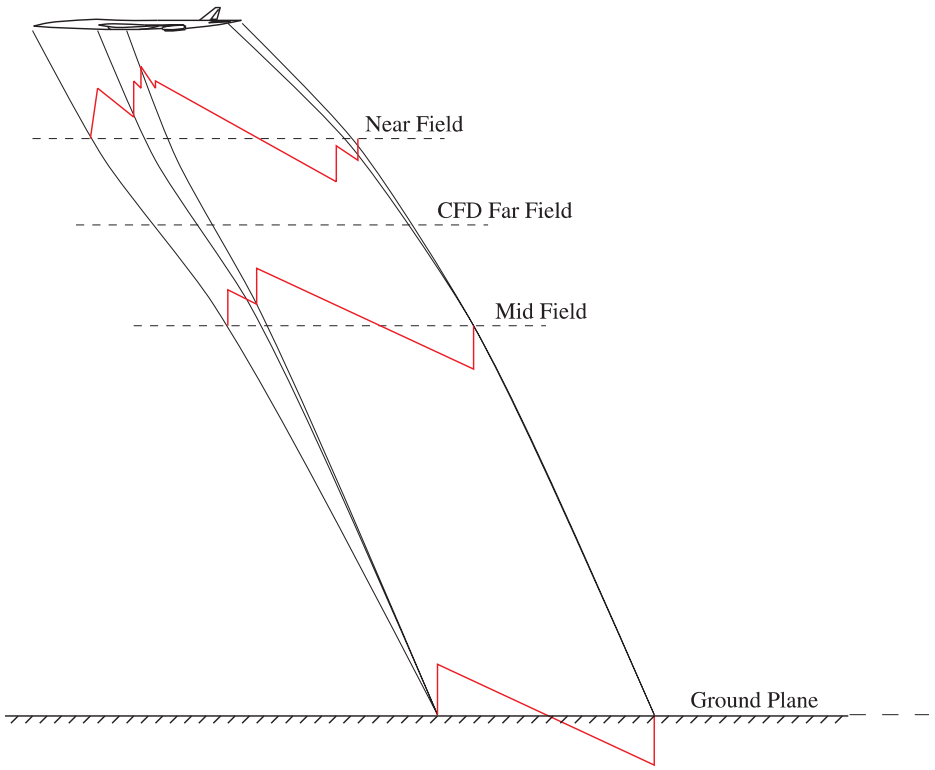

Figure 1. Schematic of the propagation of the aircraft pressure signature.

are a selected number of papers on this topic. Orr et al. (2002) proposed a rather exotic concept to reduce the sonic boom. Their goal was to increase the apparent length of the aircraft by off-axis volume addition. A swept forward keel placed normal to the Mach plane increased the apparent length and proved to be effective in reducing the sonic boom strength. Komadina et al. (2002) evaluated twelve different configurations. The ground sonic boom signature, aircraft aerodynamics, mass properties, and flight performance were evaluated for all twelve configurations using empirical methods. The two most promising concepts were then chosen and higher fidelity methods were used to compute the vehicle performance and characteristics. Argrow et al. (2002) argued that most sonic boom minimization techniques shape the aircraft equivalent body of revolution in the vertical plane and not the true geometry to reduce the far-field pressure signatures. The authors used a combination of linearized and non-linear aerodynamic theories, computational fluid dynamics based on the Euler equations, and a gradient-based method to optimize the shape of the aircraft. The design variables were nose tilt angle and canard and wing dihedral, sweep, and twist angles.

Through the support of the DARPA QSP Program, advanced algorithms for the design and optimization of quiet supersonic platforms have been developed during the last several years. DARPA's vision for the project was to develop conceptual aircraft designs that produced initial overpressures of 0.3 psf (1 psf = 4.88243 kg/m^2), while cruising at Mach 2.5 with a range of 6000 nautical miles and with a weight around 100 000 lbs (1 lb = 4.53592×10^{-1} kg). This is an ambitious reduction in the initial overpressure compared to the Concorde's 1.5–2.0 psf. Our experience has indicated that large reductions in the ground peak pressure cannot be achieved with minor shape modifications of the baseline configuration. Alternative design methods such as genetic algorithms have been used in a multi-level design environment to reach the neighborhood of the optimum design before switching over to a gradient-based method to refine the design. Promising results have been achieved by using genetic algorithms in a linear method environment. Non-linear methods are needed to meet several goals: first, to verify if not improve the results of the linear-based method; second, to improve the design by using the techniques of optimal control; lastly, to allow the introduction of more objective functions to improve the final design.

The concept presented in this work proposes the idea that the ground pressure signature could be adjusted by modifying the aircraft surface geometry to control the near-field pressure distribution. It is not at all clear what type of changes to the surface geometry would produce near-field pressure distributions whose propagation to the ground would generate sonic booms with lower peaks. It appears, however, that the problem might be separated into two parts: first, the identification of near-field pressure distributions that are both feasible and lead to acceptable ground signatures; and second, the design of the surface geometry such that it will produce the desired near-field pressure distribution.

Traditional adjoint implementations have been aimed at reducing a cost function computed from the pressure distribution on the surface that is being modified. In this case,

however, we would like to obtain the sensitivity of pressure distributions at points located at a distance from the surface where the geometry is being modified. This type of sensitivity calculation has not been attempted before in aerodynamic shape design, but is closely related to inverse-scattering problems in acoustics and electromagnetics. In such an approach, a target near-field pressure distribution must be specified. The cost function may then be chosen as the integral of the square of the difference between the current and target near-field pressure distribution. The gradient of the cost function with respect to the design variables such as the position of the surface mesh points is calculated, and a direction of improvement is obtained from an optimization algorithm. The procedure is repeated until a new aircraft surface geometry is produced that provides a near-field pressure signature that approaches the specified target near field pressure distribution, provided that it is actually realizable. The design procedure should also include other objective functions and constraints to maintain or improve other aircraft performance parameters such as lift-to-drag ratio and the total amount of lift. The possibility that the adjoint method could be adapted to solve the remote inverse problem was demonstrated by Nadarajah et al. (2001) for a two-dimensional internal flow problem. The method was then extended for three-dimensional wing and wing–body configurations in supersonic flow by Nadarajah et al. (2002a, 2002b, 2002c).

The issue of choosing a near-field signature to produce a desired ground signature was addressed by Alonso et al. (2002). The work accomplished in this research focuses on controlling the near field signature, and not the ground signature. A future extension of the method would be to include the wave propagation program in the design procedure, such that the ground pressure signature is considered as the target pressure distribution instead of the near-field pressure distribution.

The Remote Inverse Design Problem Using Control Therapy

The aerodynamic properties that define the cost function are functions of the flow field variables, w, and the physical location of the boundary, which may be represented by the function $\mathcal{S}$.

Suppose that the performance is measured by a cost function

$$I = \varpi_1 \int_{\mathcal{B}_W} \mathcal{M}(w, \mathcal{S})\, \mathrm{d}\mathcal{B}_\xi + \varpi_2 \int_{\mathcal{B}_{NF}} \mathcal{N}(w, \mathcal{S})\, \mathrm{d}\mathcal{B}_\xi \qquad (1)$$

containing both wall boundary ($\mathcal{B}_W$) and near field boundary ($\mathcal{B}_{NF}$) contributions, where $\mathrm{d}\mathcal{B}_\xi$ includes the surface and near-field elements in the computational domain, while ϖ_1 and ϖ_2 are the weighting coefficients. The coordinates ξ_i that describe the fixed computational domain are chosen so that each boundary conforms to a constant value of one of these coordinates. In general, $\mathcal{M}$ and $\mathcal{N}$ will depend on both the flow variables w and the metrics $\mathcal{S}$ defining the computational space.

The design problem is now treated as a control problem where the boundary shape represents the control function, which is chosen to minimize I subject to the constraints defined by the flow equations. A shape change produces a variation in the flow solution, δw, and the metrics, $\delta\mathcal{S}$, which in turn produce a variation in the cost function

$$\delta I = \varpi_1 \int_{\mathcal{B}_W} \delta\mathcal{M}(w, \mathcal{S})\, \mathrm{d}\mathcal{B}_\xi + \varpi_2 \int_{\mathcal{B}_{NF}} \delta\mathcal{N}(w, \mathcal{S})\, \mathrm{d}\mathcal{B}_\xi \qquad (2)$$

with $\delta\mathcal{M} = [\mathcal{M}_w]_{\mathcal{I}}\, \delta w + \delta\mathcal{M}_{\mathcal{II}}$, $\delta\mathcal{N} = [\mathcal{N}_w]_{\mathcal{I}}\, \delta w + \delta\mathcal{N}_{\mathcal{II}}$, where we use the subscripts $\mathcal{I}$ and $\mathcal{II}$ to distinguish between the contributions associated with the variation of the flow solution δw and those associated with the metric variations $\delta\mathcal{S}$. Thus, $[\mathcal{M}_w]_{\mathcal{I}}$ and $[\mathcal{N}_w]_{\mathcal{I}}$ represent $\partial\mathcal{M}/\partial w$ and $\partial N/\partial w$ with the metrics fixed, while $\delta\mathcal{M}_{\mathcal{II}}$ and $\delta\mathcal{N}_{\mathcal{II}}$ represent the contribution of the metric variations $\delta\mathcal{S}$ to $\delta\mathcal{M}$ and $\delta\mathcal{N}$ with the flow solution fixed. The weak form of the Euler equations for steady flow is

$$\int_{\mathcal{D}} \frac{\partial \psi^{\mathrm{T}}}{\partial \xi_i} \delta F_i\, \mathrm{d}\mathcal{D} = \int_{\mathcal{B}} n_i \psi^{\mathrm{T}} \delta F_i\, \mathrm{d}\mathcal{B}$$

where the test vector ψ is an arbitrary differentiable function, and n_i is the outward normal at the boundary. If a differentiable solution, w, for this equation is obtained, then it can be integrated by parts to give

$$\int_{\mathcal{D}} \psi^{\mathrm{T}} \frac{\partial}{\partial \xi_i} \delta F_i\, \mathrm{d}\mathcal{D} = 0 \qquad (3)$$

Since this is true for any ψ, the differential form can be recovered. Here, δF_i can be split into contributions associated with δw and $\delta\mathcal{S}$ using a similar notation

$$\delta F_i = [F_{iw}]_{\mathcal{I}}\, \delta w + \delta F_{i\mathcal{II}} \quad \text{where} \quad [F_{iw}]_{\mathcal{I}} = S_{ij} \frac{\partial f_j}{\partial w}$$

The domain can then be split into two parts as shown in **Figure 2**. First, the near-field domain ($\mathcal{D}_1$) whose boundaries are the wing surface and the near-field boundary plane. Second, the far-field domain ($\mathcal{D}_2$), which borders the near-field domain along the near-field boundary plane and the far-field boundary. Thus equation (3) can be written as

$$\int_{\mathcal{D}_1} \psi^{\mathrm{T}} \frac{\partial}{\partial \xi_i} \delta F_i\, \mathrm{d}\mathcal{D}_\xi + \int_{\mathcal{D}_2} \psi^{\mathrm{T}} \frac{\partial}{\partial \xi_i} \delta F_i\, \mathrm{d}\mathcal{D}_\xi = 0$$

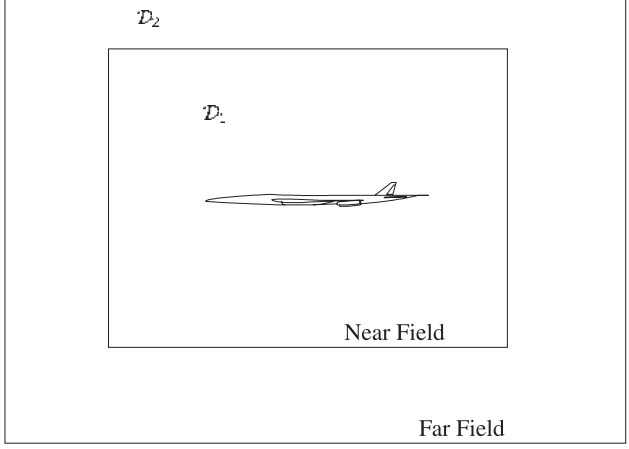

Figure 2. Near-field and far-field domains.

This may be integrated by parts to give

$$\int_{\mathcal{B}_W} n_i \psi^T \delta F_i \, d\mathcal{D}_\xi - \int_{\mathcal{D}_1} \frac{\partial \psi^T}{\partial \xi_i} \delta F_i \, d\mathcal{D}_\xi$$

$$+ \int_{\mathcal{B}_{NF}} n_i (\psi^+ - \psi^-)^T \delta F_i \, d\mathcal{D}_\xi - \int_{\mathcal{D}_2} \frac{\partial \psi^T}{\partial \xi_i} \delta F_i \, d\mathcal{D}_\xi = 0 \qquad (4)$$

where ψ^+ and ψ^- are the values of the Lagrange Multiplier, ψ, above and below the boundary. Since the left-hand expression equals zero, it may be subtracted from the variation in the cost function (2) to give

$$\delta I = \int_{\mathcal{B}_W} [\varpi_1 \delta \mathcal{M} - n_i \psi^T \delta F_i] d\mathcal{B}_\xi + \int_{\mathcal{B}_{NF}} [\varpi_2 \delta \mathcal{N} - n_i (\psi^+ - \psi^-)^T \delta F_i] d\mathcal{B}_\xi + \int_{\mathcal{D}_1} \frac{\partial \psi^T}{\partial \xi_i} \delta F_i \, d\mathcal{D}_\xi + \int_{\mathcal{D}_2} \int_{\mathcal{D}_1} \frac{\partial \psi^T}{\partial \xi_i} \delta F_i \, d\mathcal{D}_\xi \qquad (5)$$

Since ψ is an arbitrary differentiable function, it may be chosen in such a way that δI no longer depends explicitly on the variation of the state vector δw. The gradient of the cost function can then be evaluated directly from the metric variations without having to re-compute the variation δw resulting from the perturbation of each design variable.

Comparing equations (2) and (4), the variation δw may be eliminated from Equation (5) by equating all field terms with subscript $\mathcal{I}$ to produce a differential adjoint system governing ψ

$$\left[\frac{\partial \psi^T}{\partial \xi_i} [F_{iw}]_{\mathcal{I}} \right]_{\mathcal{D}_1 + \mathcal{D}_2} = 0 \text{ in } \mathcal{D} \qquad (6)$$

The corresponding wall and near-field adjoint boundary conditions are produced by equating the subscript $\mathcal{I}$ boundary terms in equation (5) to produce

$$n_i \psi^T [F_{iw}]_{\mathcal{I}} = \varpi_1 \mathcal{M}_w \quad \text{on} \quad \mathcal{B}_W \qquad (7)$$

$$n_i (\psi^+ - \psi^-)^T [F_{iw}]_{\mathcal{I}} = \varpi_2 \mathcal{N}_w \quad \text{on} \quad \mathcal{B}_{NF} \qquad (8)$$

The remaining terms from equation (5) then yield a simplified expression for the variation of the cost function, which defines the gradient

$$\delta I = \int_{\mathcal{B}_W} \{\varpi_1 \delta \mathcal{M}_{\mathcal{II}} - n_i \psi^T [\delta F_i]_{\mathcal{II}}\} d\mathcal{B}_\xi + \int_{\mathcal{B}_{NF}} \{\varpi_2 \delta \mathcal{N}_{\mathcal{II}} - n_i (\psi^+ - \psi^-)^T [\delta F_i]_{\mathcal{II}}\} d\mathcal{B}_\xi + \int_{\mathcal{D}_1 + \mathcal{D}_2} \left\{ \frac{\partial \psi^T}{\partial \xi_i} [\delta F_i]_{\mathcal{II}} \right\} d\mathcal{D}_\xi \qquad (9)$$

The details of the formula for the gradient depend on the way in which the boundary shape is parameterized as a function of the design variables and the way in which the mesh is deformed as the boundary is modified. The boundary conditions satisfied by the flow equations restrict the form of the left-hand side of the adjoint boundary conditions (7) and (8). Consequently, the boundary contribution to the cost functions $\mathcal{M}$ and $\mathcal{N}$ cannot be specified arbitrarily. Instead it must be chosen from the class of functions that allow cancellation of all terms containing δw in the boundary integral of equation (5). In this research, the cost function is the weighted sum of the drag coefficient and the Sobolev norm of the difference between the current and target remote pressure distributions. From equation (1), $\mathcal{M}$ and $\mathcal{N}$ can be defined as

$$\mathcal{M}(w, \mathcal{S}) = \frac{1}{c} C_p \left(\frac{\partial y}{\partial \xi} \cos\alpha - \frac{\partial x}{\partial \xi} \sin\alpha \right)$$

and

$$\mathcal{N}(w, \mathcal{S}) = \frac{1}{2} (p - p_T)^2$$

The cost function can then be written as

$$I = \varpi_1 \frac{1}{c} \int_{\mathcal{B}_W} C_p \left(\frac{\partial y}{\partial \xi} \cos\alpha - \frac{\partial x}{\partial \xi} \sin\alpha \right) d\mathcal{B}_\xi + \varpi_2 \frac{1}{2} \int_{\mathcal{B}_{NF}} (p - p_T)^2 \, d\mathcal{B}_\xi$$

and further simplified to

$$I = \varpi_1 C_D + \varpi_2 \frac{1}{2}\int_{\mathcal{B}_{NF}} (p - p_T)^2 \, d\mathcal{B}_\xi \tag{10}$$

The values of the weighting coefficients are selected based on the relative magnitude of the gradients of the drag minimization and the remote inverse cost functions. The remote inverse gradient is typically an order of magnitude smaller than the gradient due to drag minimization. Therefore, the weights are chosen to increase the magnitude of the gradient from the remote inverse cost function. In practice, larger weights are used for the remote inverse gradient, since the primary design objective is to reduce the near-field pressure signature. The disadvantage of this approach is that the weights must be chosen at the beginning of the design process and if the user does not have prior knowledge of the magnitude of the gradients, then generally an initial guess is taken. The weights are altered for subsequent runs.

An alternative method for problems with more than one objective function is to develop separate adjoint equations, one for each objective function. Both gradients are then calculated separately, multiplied by weights, and summed. A direction of improvement is then based on the new gradient. This method has the advantage that the user is better equipped with knowledge regarding the difference in magnitude between the two gradients. Appropriate weights are chosen to achieve the desired compromise. A disadvantage is the need to calculate a separate adjoint solution for each objective function.

In this work, we prefer to use a composite cost function, since we had a priori knowledge regarding the magnitude of the gradient contribution from the remote inverse and the drag minimization cost functions.

Remote Inverse Design via the Discrete Adjoint Method

The remote inverse adjoint method can be formulated either by the continuous or discrete adjoint method. The previous section offers an overview of the continuous adjoint approach. The continuous remote adjoint boundary condition would require an update of the adjoint variables at the near-field cells. Since the near-field cells, do not lie in a specific row or column of cells in the vicinity of the near field, but rather as a group of cells scattered along the near-field plane, the implementation of the continuous adjoint approach would prove to be far to complex. However, the discrete adjoint approach proved to be less complicated, and offered a manageable approach to the implementation of the remote adjoint boundary condition problem.

The discrete adjoint equation is obtained by applying control theory directly to the set of discrete field equations. To formulate the discrete adjoint equation, we first define the cost function I as such,

$$I = \varpi_1 C_D + \varpi_2 \frac{1}{2}\sum_{NF} (p - p_T)^2 \, \Delta s$$

where C_D is total wing drag coefficient, p is the current near field pressure, and p_T is the target near-field pressure. Next, we take a variation of the residual term, which can be written as

$$\delta R(w)_{i,j,k} = \delta h_{i+\frac{1}{2},j,k} - \delta d_{i-\frac{1}{2},j,k} + \delta h_{i,j+\frac{1}{2},k} - \delta h_{i,j-\frac{1}{2},k} + \delta h_{i,j,k+\frac{1}{2}} - \delta h_{i,j,k-\frac{1}{2}} \tag{11}$$

with $\delta h_{i+1/2,j,k} = \delta f_{i+1/2,j,k} - \delta d_{i+1/2,j,k}$, where f is the convective flux and d is the artificial dissipation flux. We then pre-multiply the variation of the discrete residual by the Lagrange Multiplier and sum the product over the computational domain to produce the following:

$$\sum_{i=2}^{i_{max}} \sum_{j=2}^{j_{max}} \sum_{k=2}^{k_{max}} \psi^T_{i,j,k} \, \delta R(w)_{i,j,k}$$

The variation of the cost function, δI, can then be augmented by the product of the variation of the discrete governing equation and the Lagrange Multiplier $\psi^T_{i,j,k}$.

$$\delta I = \varpi_1 \delta C_D + \varpi_2 \sum_{NF} (p - p_T)\, \delta p \, \Delta s + \sum_{i=2}^{i_{max}} \sum_{j=2}^{j_{max}} \sum_{k=2}^{k_{max}} \psi^T_{i,j,k} \, \delta R(w)_{i,j,k} \tag{12}$$

To eliminate δw from equation (12), terms multiplied by the variation $\delta w_{i,j,k}$ of the discrete flow variables are collected and equated to zero. The following is the resulting discrete adjoint equation:

$$V = \frac{\partial \psi_{i,j}}{\partial t} = \frac{1}{2}\Bigg[\left(S_{11}{}_{i-\frac{1}{2},j,k} A1^{\mathrm{T}}_{i,j,k} + S_{12}{}_{i-\frac{1}{2},j,k} A2^{\mathrm{T}}_{i,j,k} + S_{13}{}_{i-\frac{1}{2},j,k} A3^{\mathrm{T}}_{i,j,k} \right)(\psi_{i,j,k} - \psi_{i-1,j,k})$$

$$+ \left(S_{11}{}_{i+\frac{1}{2},j,k} A1^{\mathrm{T}}_{i,j,k} + S_{12}{}_{i+\frac{1}{2},j,k} A2^{\mathrm{T}}_{i,j,k} + S_{13}{}_{i+\frac{1}{2},j,k} A3^{\mathrm{T}}_{i,j,k} \right)(\psi_{i+1,j,k} - \psi_{i,j,k})$$

$$+ \left(S_{21}{}_{i,j+\frac{1}{2},k} A1^{\mathrm{T}}_{i,j,k} + S_{22}{}_{i,j+\frac{1}{2},k} A2^{\mathrm{T}}_{i,j,k} + S_{23}{}_{i,j+\frac{1}{2},k} A3^{\mathrm{T}}_{i,j,k} \right)(\psi_{i,j+1,k} - \psi_{i,j,k})$$

$$+ \left(S_{21}{}_{i,j-\frac{1}{2},k} A1^{\mathrm{T}}_{i,j,k} + S_{22}{}_{i,j-\frac{1}{2},k} A2^{\mathrm{T}}_{i,j,k} + S_{23}{}_{i,j-\frac{1}{2},k} A3^{\mathrm{T}}_{i,j,k} \right)(\psi_{i,j,k} - \psi_{i,j-1,k})$$

$$+ \left(S_{31}{}_{i,j,k+\frac{1}{2}} A1^{\mathrm{T}}_{i,j,k} + S_{32}{}_{i,j,k+\frac{1}{2}} A2^{\mathrm{T}}_{i,j,k} + S_{33}{}_{i,j,k+\frac{1}{2}} A3^{\mathrm{T}}_{i,j,k} \right)(\psi_{i,j,k+1} - \psi_{i,j,k})$$

$$+ \left(S_{31}{}_{i,j,k-\frac{1}{2}} A1^{\mathrm{T}}_{i,j,k} + S_{32}{}_{i,j,k-\frac{1}{2}} A2^{\mathrm{T}}_{i,j,k} + S_{33}{}_{i,j,k-\frac{1}{2}} A3^{\mathrm{T}}_{i,j,k} \right)(\psi_{i,j,k} - \psi_{i,j,k-1})$$

$$+ \mathcal{D}_{i+\frac{1}{2},j,k} - \mathcal{D}_{i-\frac{1}{2},j,k} + \mathcal{D}_{i,j+\frac{1}{2},k} - \mathcal{D}_{i,j-\frac{1}{2},k} + \mathcal{D}_{i,j,k+\frac{1}{2}} - \mathcal{D}_{i,j,k-\frac{1}{2}} \tag{13}$$

Here, V is the cell area and

$$\mathcal{D}_{i+\frac{1}{2},j,k} = \nu^2_{i+\frac{1}{2}j,k} \Lambda_{i+\frac{1}{2},j,k}(\psi^{\mathrm{T}}_{i+1,j,k} - \psi^{\mathrm{T}}_{i,j,k}) - \nu^{(4)}_{i+\frac{3}{2}j,k} \Lambda_{i+\frac{3}{2},j,k}(\psi^{\mathrm{T}}_{i+2,j,k} - \psi^{\mathrm{T}}_{i+1,j,k})$$
$$+ 2\nu^{(4)}_{i+\frac{1}{2}j,k} \Lambda_{i+\frac{1}{2},j,k}(\psi^{\mathrm{T}}_{i+1,j,k} - \psi^{\mathrm{T}}_{i,j,k}) - \nu^{(4)}_{i-\frac{1}{2}j,k} \Lambda_{i-\frac{1}{2},j,k}(\psi^{\mathrm{T}}_{i,j,k} - \psi^{\mathrm{T}}_{i-1,j,k})$$

is the discrete adjoint artificial dissipation term that corresponds to the discretization of the inviscid flow equations by the Jameson–Schmidt–Turkel (JST) scheme (1981). The dissipation coefficients $\nu^{(2)}$ and $\nu^{(4)}$ are functions of the flow variables, but, to reduce complexity, they are treated as constants. The effect of this partial discretization has been explored by Nadarajah and Jameson (2000, 2001).

Discrete Adjoint Boundary Condition

To develop the discrete adjoint boundary condition for the calculation of remote sensitivities for supersonic flow, the δw_{NF} term from the discrete cost function is added to the corresponding term from equation (12). The discrete boundary condition appears as a source term in the adjoint fluxes. At the NF cell, the source term Φ_{NF} for inverse design is added to equation (13) and can be written as,

$$\Phi_{\mathrm{NF}} = -\varpi_1(p - p_{\mathrm{T}})\,\Delta s_{\mathrm{NF}}\,\delta p_{\mathrm{NF}}$$

The wall boundary condition appears as source terms in the adjoint fluxes along the cells above the wall. The derivation of this boundary condition was explored by Nadarajah and Jameson (2000). For a first-order dissipation scheme, the discrete adjoint equations are completely independent of the co-state variables in the cells below the wall. However, if we use the blended first-and-third-order scheme, these flow variable values are required. A simple zeroth-order extrapolation across the wall has produced good results, as shown by Nadarajah and Jameson (2000).

Optimization Procedure

In this paper, the inverse design boundary condition is applied to the near field, while sensitivity derivatives or the gradient are calculated on the airfoil surface. The gradient for the discrete adjoint is obtained by perturbing each point on the lower wall. Once the gradient $\mathcal{G}$ has been determined, it can be used to drive a variety of gradient-based search procedures. The search procedure used in this work is a descent method in which small steps are taken in the negative gradient direction. Let $\mathcal{F}$ represent the design variable, and $\mathcal{G}$ the gradient. Then an improvement can be made with a shape change

$$\delta\mathcal{F} = -\lambda\mathcal{G}$$

However, it is better to replace the gradient $\mathcal{G}$ by a smoothed value $\overline{\mathcal{G}}$ in the descent process. This acts as a preconditioner that allows the use of much larger steps and ensures that each new shape in the optimization sequence remains smooth. To apply smoothing in the ξ_1 direction, the smoothed gradient $\overline{\mathcal{G}}$ may be calculated from a discrete approximation to

$$\overline{\mathcal{G}} - \frac{\partial}{\partial \xi_1}\theta\frac{\partial \overline{\mathcal{G}}}{\partial \xi_1} = \mathcal{G}, \qquad \overline{\mathcal{G}} = 0 \quad \text{at end points}$$

where θ is the smoothing parameter. If the modification is applied on the surface ξ_2 = constant, then the first-order change in the cost function is

$$\begin{aligned}\delta I &= -\int\int \mathcal{G}\,\delta\mathcal{F}\,\mathrm{d}\xi_1 \\ &= -\lambda\int\int\left(\overline{\mathcal{G}} - \frac{\partial}{\partial\xi_1}\theta\frac{\partial}{\partial\xi_1}\overline{\mathcal{G}}\right)\overline{\mathcal{G}}\,\mathrm{d}\xi_1 \\ &= -\lambda\int\int\left(\overline{\mathcal{G}}^2 + \theta\left(\frac{\partial\overline{\mathcal{G}}}{\partial\xi_1}\right)^2\right)\mathrm{d}\xi_1 \\ &< 0\end{aligned}$$

again guaranteeing an improvement unless $\overline{\mathcal{G}} = \mathcal{G} = 0$ and assuring an improvement if λ is sufficiently small and positive.

In some problems, it turns out that the Hessian can be represented as a second-order differential operator, so that with a proper choice of the smoothing parameter, the method becomes the Newton method. Search methods were intensively evaluated in a recent study by Jameson and Vassberg (1999), and it was verified that these sample problems (which may have a high linear content) could be solved with a number of search steps independent of the number of design variables.

Results

This section presents the results of remote inverse and drag minimization for wing–body configurations in supersonic flow. The objective is to reduce the peak pressure at the near-field plane and thus reduce the ground signature peak. Viscous effects are likely to be very small in these examples, so it is sufficient to use the Euler equations. The calculations were performed with the new SYN88-MBC multiblock code that takes advantage of the FORTRAN 90/95 derived data type architecture. The flow solver is augmented with an adjoint solver and shape modification routines to allow for automatic shape optimization.

Wing–Body Configuration: Sonic Boom Reduction, Without Lift Constraint, Wing Redesign Only

The wing–body supersonic business jet configuration was sized to accommodate between 6 to 8 passengers with a gross take-off weight of 100 000 lbs and a fuselage length of 100 ft. The supersonic flight condition at which all designs were calculated is Mach 1.5. **Figure 3** shows the wing–body configuration. The fuselage is cylindrical and the maximum diameter occurs at 31% of the fuselage length measured from the nose. The wing is a biconvex wing with a 7.125° leading edge sweep, an aspect ratio of 3.0, and a taper ratio of 0.218. The root airfoil is a 3% thick biconvex airfoil and the tip is 1.5% thick. The biconvex profile in the center sections was obtained by interpolating between the root and tip. The airfoils were constructed to accommodate deep spars at the 10% and 80% chord locations. The baseline wing does not have geometric twist. The computational mesh has eight blocks with 193 × 49 × 33 nodes on a C–H grid. The fuselage has 25 points in the cross-streamwise-direction and 144 points in the streamwise-direction. The wing contains 97 points in the streamwise-direction and 17 sectional cuts in the spanwise-

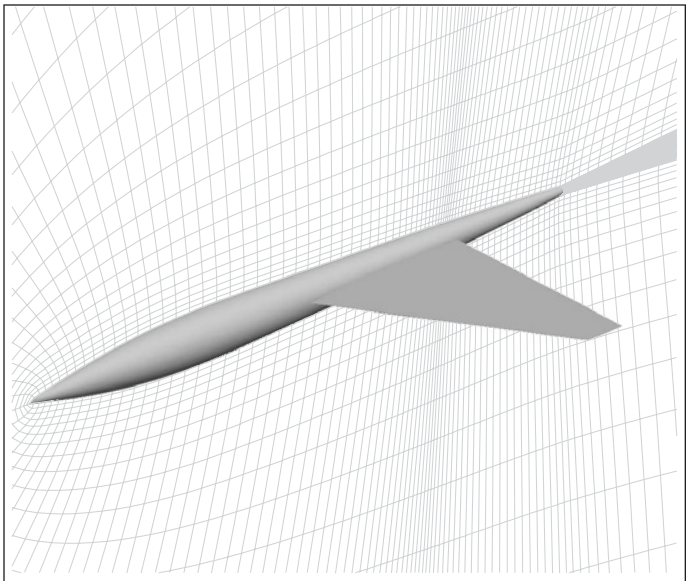

Figure 3. Business jet wing–body configuration: biconvex wing, 193×49×33 C–H grid, 8 blocks.

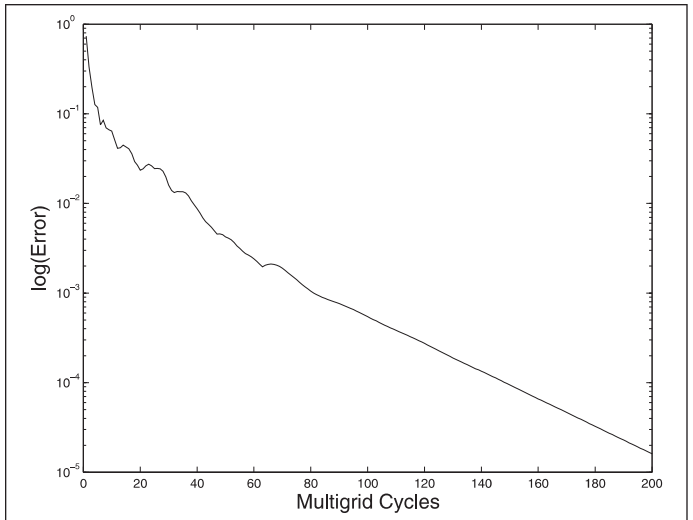

Figure 4. Convergence history of the flow solver.

direction. The far-field boundary is located at approximately 5 root chord lengths. In **Figure 4**, convergence history of the flow solver is illustrated for the Mach 1.5 test case.

To obtain an accurate representation of the far-field pressure signature through a wave propagation method, a precise near-field pressure distribution must be acquired. The location of the near-field boundary is largely influenced by the number of mesh points. A large number of mesh points would result in smaller mesh spacings in the region of the near field and produce a pressure distribution of greater accuracy, however, the computational cost would increase dramatically. If located too close to the aircraft, a proper far-field representation of the aircraft pressure signature may not be feasible. In this work, the near-field boundary is located at approximately one root chord length below the aircraft on the 193 × 49 × 33 C–H mesh.

To illustrate the possibility of sonic boom reduction, a target pressure distribution was obtained by re-scaling the initial near-field pressure distribution. Ultimately, this step will be replaced by a method that produces a target near-field pressure based upon the desired ground pressure signature. The target pressure was obtained by taking the result of SYN88-MBC at a flight condition of M_∞ = 1.5 and scaling the resulting pressure distribution to 40% of its original value.

The objective function is the integral of the difference between the current and target near-field pressures. The minimum permissible thickness constraint is imposed at each chordwise cut between the 10% and 80% chord locations at the end of each design cycle. Points from the leading edge upto the 10% chord location and from the 80% chord location to the trailing edge are not constrained and free to move in any direction. The lift coefficient in this case is not constrained. In this design, the design variables are the locations of all of the points on the surface of the wing. Therefore, only the second peak in the near-field pressure profile will be expected to change. The flow is calculated at Mach 1.5 at a fixed angle of attack of 1.62°.

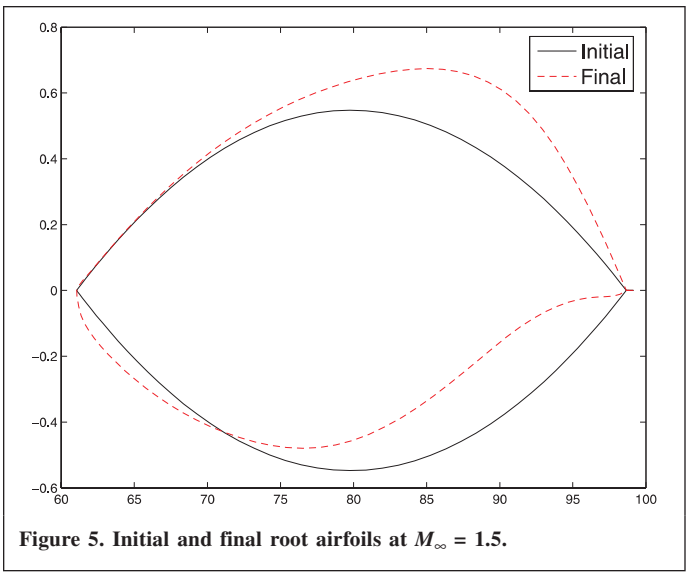

Figure 5. Initial and final root airfoils at M_∞ = 1.5.

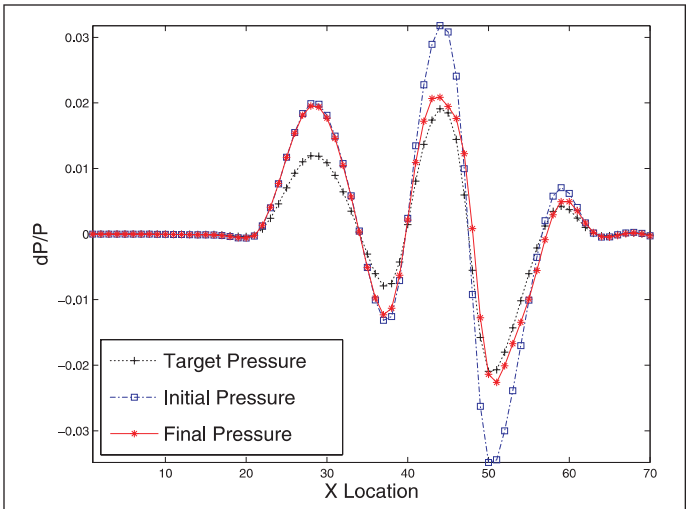

Figure 6. Target, initial, and final near-field pressure distribution after 50 design cycles.

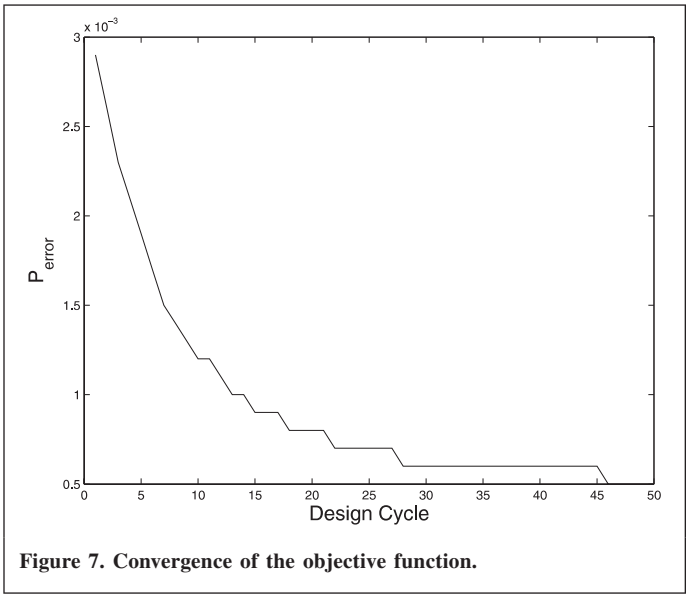

Figure 7. Convergence of the objective function.

Figure 5 illustrates the initial and final root airfoil profiles. The lower surface of the final airfoil contains a slightly larger expansion region when compared with the original biconvex airfoil. It is this modification that allows the near-field wing peak pressure (second peak) to be reduced. The larger expansion region weakens the strength of the leading edge attached shock in the near-field region. **Figure 6** shows the initial near-field pressure in blue (□) and the target pressure in black (+). After 50 design cycles, the final near-field pressure distribution is obtained and illustrated as the red (*) line. The wing peak pressure has been reduced by 40%. The large modifications on the wing upper surface are a result of the thickness constraint. Since the lift coefficient was not constrained, C_L reduced from 0.1 to 0.073. The baseline wing drag coefficient is 0.00568 and the final wing drag increased slightly to 0.00582. Even if drag due to lift has decreased due to

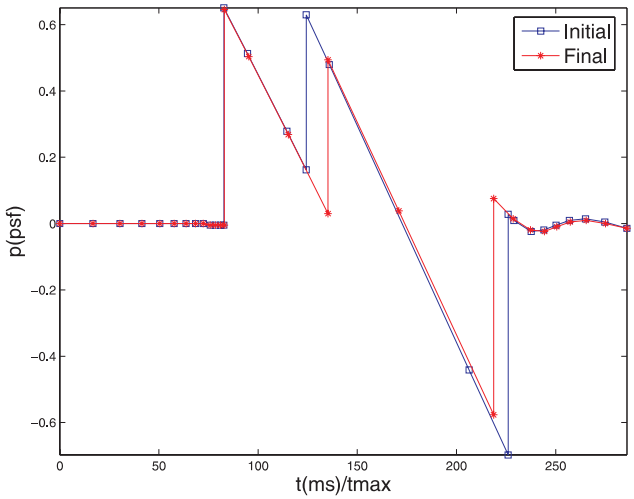

Figure 8. Initial and final ground signatures after 50 design cycles.

the decrease in the lift coefficient, the stronger attached leading edge shock has increased the wing wave drag.

In **Figure 7**, the convergence of the objective function is shown. Here, the objective function as defined in equation (10) is computed at each design cycle. For this test case, ϖ_1 is set to zero and thus the objective function only represents the norm of the difference between the current and target near-field pressure. The near-field pressure quickly reaches the vicinity of the final result within 20 design cycles. A total of 50 design cycles are computed to ensure that the objective function has reached its minimum value.

The complete shape optimization procedure for sonic boom reduction requires the determination of desirable ground boom signatures. In **Figure 8**, we show the initial and final ground signature profiles. The PC Boom software for far-field propagation developed by Wyle Associates was used to calculate the ground signatures. The results clearly indicate that arbitrarily scaled near-field signatures may not result in more desirable behavior at the ground.

Wing–Body Configuration: Sonic Boom Reduction, Lift Constraint

We now repeat the same design case but with the following three changes: first, the lift coefficient is constrained at 0.1. Second, gradients are calculated for points on the surface of the fuselage and thus allowed to be modified. Third, the objective function is the weighted sum of the drag coefficient and integral of the difference between the current and target near-field pressures, where ϖ_1 is the weight on the drag coefficient and ϖ_2 is the weight on the remote inverse cost function. In this case, the drag coefficient weight is, $\varpi_1 = 0.005$ and the remote inverse cost function weight is set to $\varpi_2 = 1$.

The value of the lift coefficient is maintained by adjusting the angle of attack to attain the desired lift coefficient of 0.1. The wing thickness constraint is imposed in the same manner as the previous case.

Figure 9 illustrates the baseline and optimized airfoil. **Figure 10** shows the target, initial, and final near-field pressure distributions. The desired target pressure distribution is not achieved in contrast with the unconstrained case illustrated in **Figure 6**. In this case, there is a struggle between the near-field peak pressure reduction versus maintenance of constant lift. Each design cycle, produces a shape modification that shifts the near-field pressure distribution towards the target pressure. Unfortunately, this also causes a reduction in the lift coefficient. This must be compensated by an increase in the angle of attack to maintain the total lift coefficient, which in turn leads to an increase in the near-field peak pressure. After 50 design cycles, the solution converges to the (*) line in **Figure 10**. The final fuselage peak pressure has been reduced to almost 18% its original value and the wing peak pressure is reduced by 22%.

To maintain the lift coefficient, the angle of attack was increased from 1.62° to 2.39°. The wing drag increased slightly

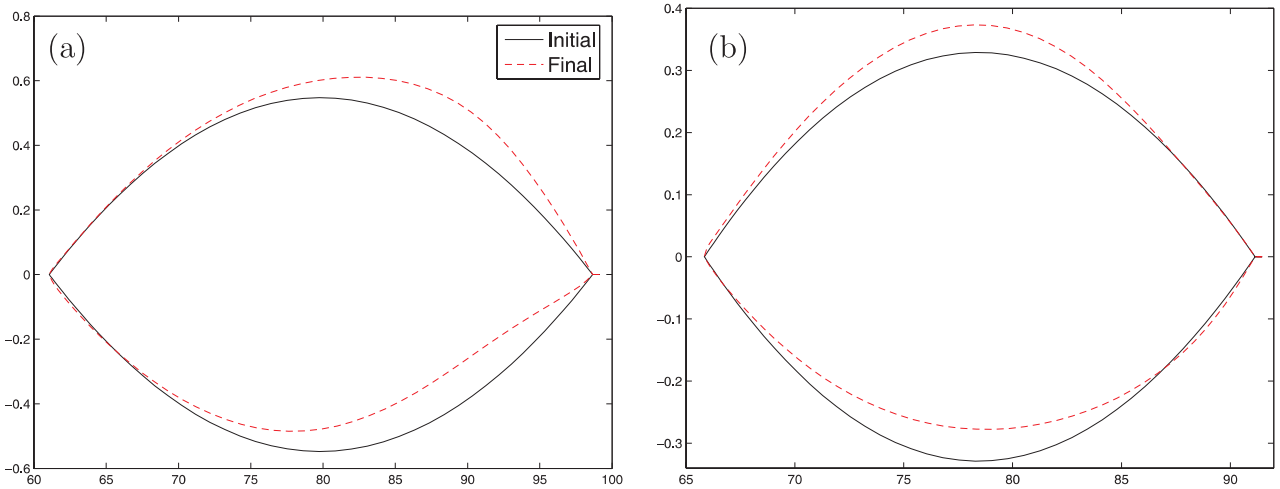

Figure 9. Initial and final root airfoils at M_∞ = 1.5. (a) Wing root section and (b) mid-span section.

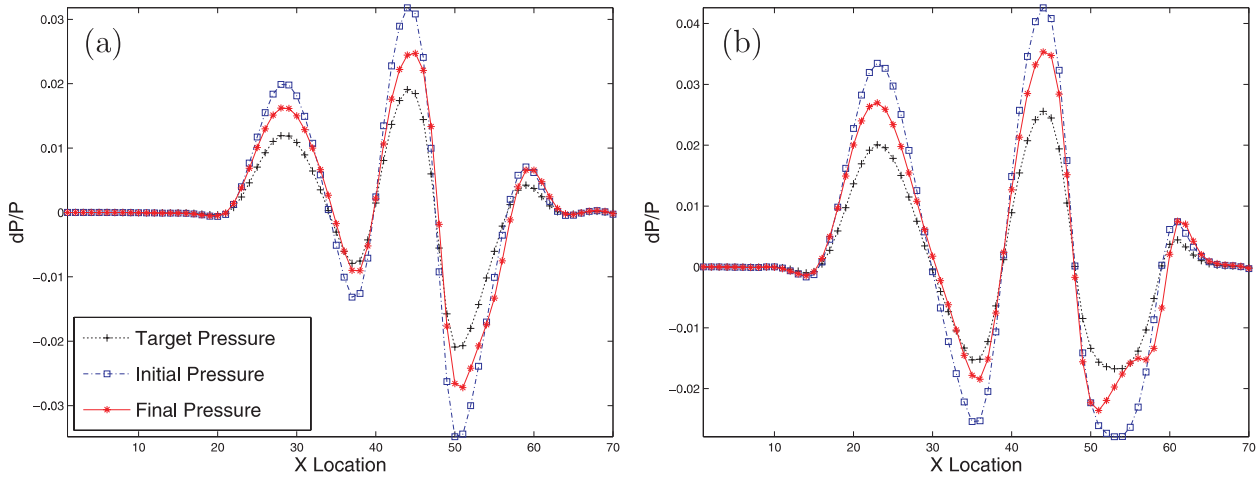

Figure 10. Target, initial, and final near-field pressure distribution after 50 design cycles. (a) Wing root section and (b) mid-span section.

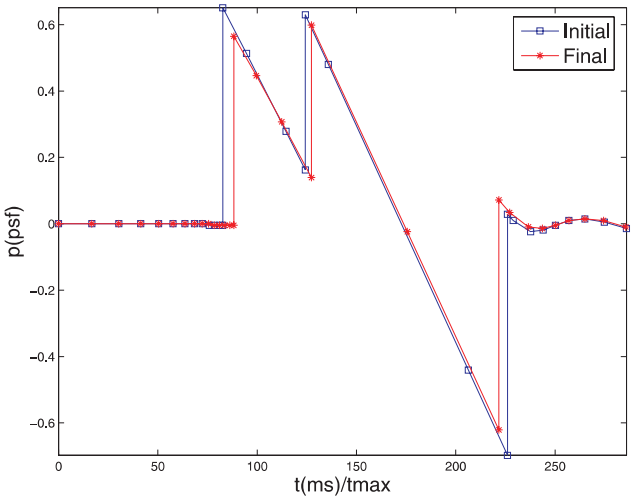

Figure 11. Sonic boom reduction: initial and final ground signatures after 50 design cycles. M_∞ = 1.5, α = 2.39°, C_L = 0.1.

Table 1. Near field peak pressure reduction and wing drag coefficient for various design cases.

Case	Fuselage peak reduction	Wing peak reduction	Wing, C_D
Baseline			0.00568
Remote inverse	18%	25%	0.00610
Drag and remote inverse	18%	22%	0.00574

from 0.00568 to 0.00574. In an alternate test case, where the drag coefficient weight was set to zero, the near-field peak pressure for both the fuselage and wing were reduced by 18% and 25%, however, the wing drag coefficient increased to 0.00610. **Table 1** contains a comparison of the two design cases. **Table 1** clearly shows that a cost function that does not include the drag coefficient will result in larger reductions in the wing near-field peak pressure. However, in a multi-disciplinary design environment, it is critical that other important parameters are kept within acceptable amounts and a trade-off between the various design goals are met. **Table 1** clearly shows that a composite cost function that includes the drag coefficient is unable to reduce both the near-field peak pressure and drag coefficient but it is able to reduce the peak pressure while maintaining the wing drag coefficient. A more detailed study of the effect of the weights on the cost functions is presented by Nadarajah et al. (2002).

In **Figure 12**, both the initial and final pressure contours are plotted. The majority of the changes in the shape are localized around the lower surface wing–fuselage intersection. The larger expansion regions on the lower surface of the wing are illustrated in these plots by the shorter red region (compression) and the longer green-orange region. This has the effect of weakening the strength of the shock, and thus reducing the peak of the near-field pressure. **Figure 13** illustrates the initial and final fuselage mesh. The larger expansion region on the underside of the fuselage around the wing–fuselage intersection is clearly due to the increase in the fuselage curvature.

Conclusions

The results presented in this paper demonstrate the feasibility of remote inverse calculations using the adjoint method. An application to the sonic boom minimization resulted in a 40% reduction in the near-field peak pressure for the unconstrained biconvex wing. In the constrained problem, the fuselage peak pressure was reduced by 18% and the wing peak by 22%. It proved highly beneficial to use a composite cost function consisting of the sum of the weighted remote inverse and drag minimization cost functions, resulting in final designs that had a reduction in the peak pressure while maintaining constant inviscid drag. Cases with no drag coefficient added to the integral of the near-field pressure

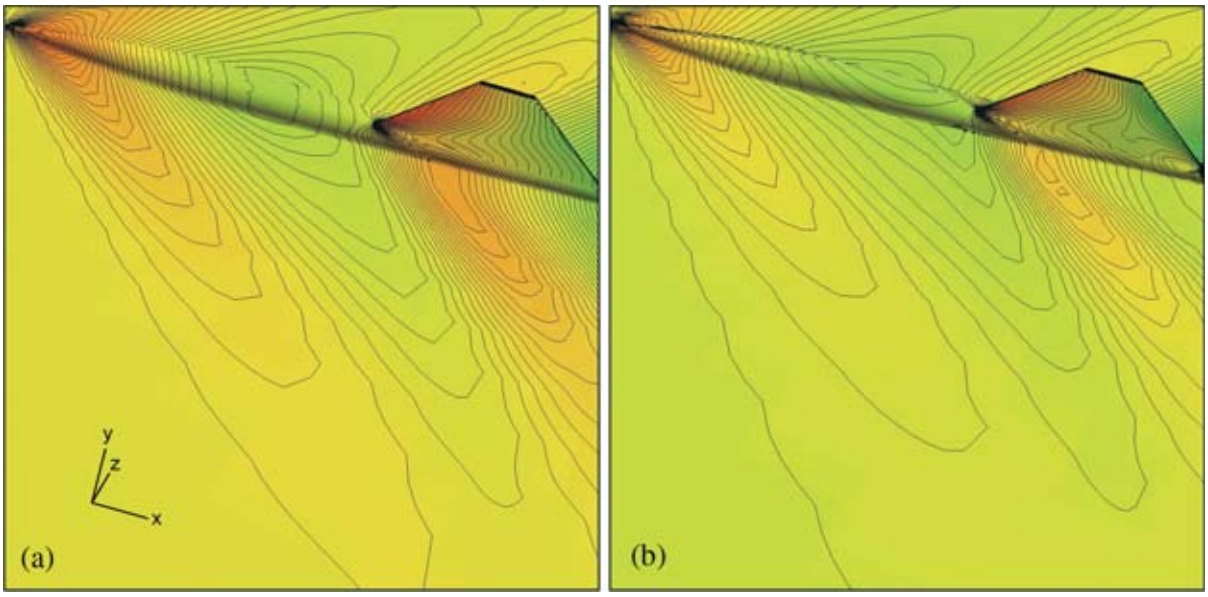

Figure 12. Pressure contour at M_∞ = 1.5. (a) Initial and (b) final.

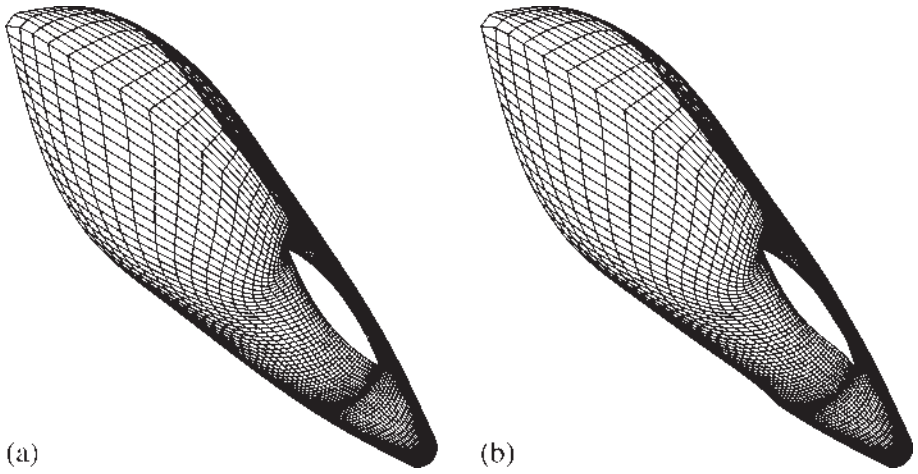

Figure 13. Fuselage mesh. (a) Initial and (b) final.

difference in the objective function saw an increase in the drag coefficient.

Acknowledgments

This research has benefited greatly from the generous support of the AFOSR under grant number AF F49620-98-1-022 and DARPA QSP Program under grant number MDA972-01-2-0003.

References

Alonso, J.J., Jameson, A., and Kroo, I. (2002). "Advanced Algorithms for Design and Optimization of Quiet Supersonic Platforms". *Proceeedings of the 40th AIAA Aerospace Sciences Meeting and Exhibit*, Reno, Nevada, 14–17 January 2002. American Institute of Aeronautics and Astronautics, Reston, Virginia. AIAA Pap. 02-0144.

Argrow, B., Farhat, C., Maute, K., and Nikbay, M. (2002). "A Shape Optimization Methodology for Reducing the Sonic Boom Initial Pressure Rise". *Proceedings of the 40th AIAA Aerospace Sciences Meeting and Exhibit*, Reno, Nevada, 14–17 January 2002. American Institute of Aeronautics and Astronautics, Reston, Virginia. AIAA Pap. 02-0145.

Cliff, S.E., Reuther, J.J., Saunders, D.A., and Hicks, R.M. (2001). "Single-point and Multipoint Aerodynamic Shape Optimization of High-Speed Civil Transport". *J. Aircr.* Vol. 38, No. 6, November-December, pp. 997–1005.

Committee on Breakthrough Technology for Commercial Supersonic Aircraft. (2001). "Commercial Supersonic Technology: The Way Ahead". National Research Council (US), National Academy Press, Washington, D.C. Tech. Rep., March.

Jameson, A., and Vassberg, J.C. (1999). "Studies of Alternative Numerical Optimization Methods Applied to the Brachistochrone Problem". OptiCON 99.

Jameson, A., Schmidt, W., and Turkel, E. (1981). "Numerical Solutions of the Euler Equations by Finite Volume Methods with Runge-Kutta Time Stepping Schemes". AIAA Pap. 81-1259, January.

Komadina, S., Drake, A., and Bruner, S. (2002). "Development of a Quiet Supersonic Aircraft with Technology Applications to Military and Civil Aircraft". *Proceedings of the 40th AIAA Aerospace Sciences Meeting and Exhibit*, Reno, Nevada, 14–17 January 2002. American Institute of Aeronautics and Astronautics, Reston, Virginia. AIAA Pap. 02-0519.

Nadarajah, S., and Jameson, A. (2000). "A Comparison of the Continuous and Discrete Adjoint Approach to Automatic Aerodynamic Optimization". *Proceedings of the 38th AIAA Aerospace Sciences Meeting and Exhibit*, Reno, Nevada, 10–13 January 2000. American Institute of Aeronautics and Astronautics, Washington, D.C. AIAA Pap. 2000-0667.

Nadarajah, S., and Jameson, A. (2001). "Studies of the Continuous and Discrete Adjoint Approaches to Viscous Automatic Aerodynamic Shape Optimization". *A Collection of Technical Papers: 15th AIAA Computational Fluid Dynamics Conference and Exhibit*, Anaheim, California, 11–14 June 2001. American Institute of Aeronautics and Astronautics, Reston, Virginia. AIAA Pap. 2001-2530.

Nadarajah, S., Jameson, A., and Alonso, J.J. (2001). "An Adjoint Method for the Calculation of Non-collocated Sensitivities in Supersonic Flow". *Proceedings of the 1st MIT Conference on Computational Fluid and Solid Mechanics*, Cambridge, Massachusetts, 12–15 June 2001. Vol. 2. Edited by K.J. Bathe. Elsevier, New York, New York. pp. 921–925.

Nadarajah, S., Jameson, A., and Alonso, J.J. (2002a). "An Adjoint Method for the Calculation of Remote Sensitivities in Supersonic Flow". *Proceedings of the 40th AIAA Aerospace Sciences Meething and Exhibit*, Reno, Nevada, 14–17 January 2002. American Institute of Aeronautics and Astronautics, Reston, Virginia. AIAA Pap. 2002-0261.

Nadarajah, S., Jameson, A., and Alonso, J.J. (2002b). "Sonic Boom Reduction using an Adjoint Method for Wing-Body Configurations in Supersonic Flow". *Proceedings of the 9th AIAA/ISSMO Symposium on Multidisciplinary Analysis and Optimization Conference*, Atlanta, Georgia, 4–6 September 2002. Vol. 2. American Institute of Aeronautics and Astronautics, Reston, Virginia. AIAA Pap. 2002-5547.

Nadarajah, S.K., Kim, S., Jameson, A., and Alonso, J.J. (2002c). "Sonic Boom Reduction using an Adjoint Method for Supersonic Transport Aircraft Configuration". *Proceedings of the IUTAM Symposium Transsonicum IV*, Göttingen, Germany, 2–6 September 2002. Edited by H. Sobieczky. Kluwer Academic Publishers, Dordrecht, The Netherlands. p. 355.

Orr, M., Mozingo, J., Marconi, F., Bowersox, R., and Schetz, J. (2002). "Sonic Boom Alleviation using Keel Configurations". *Proceedings of the 40th AIAA Aerospace Sciences Meeting and Exhibit*, Reno, Nevada, 14–17 January 2002. American Institute of Aeronautics and Astronautics, Reston, Virginia. AIAA Pap. 02-0149.

Seebass, R., and Argrow, B. (1998). "Sonic Boom Minimization Revisited". *Proceedings of the 2nd AIAA Theoretical Fluid Mechanics Meeting*, Albuquerque, New Mexico, June 1998. AIAA Pap. 98-2956.

Thomas, C. (1971). "Extrapolation of Sonic Boom Pressure Signatures by the Waveform Parameter Method". NASA TN D-6832.

Whitham, G.B. (1952). "The Flow Pattern of a Supersonic Projectile". *Commun. Pure Appl. Math.* Vol. 3, pp. 301–348.

